HHS Public Access

Author manuscript

ACS Appl Mater Interfaces. Author manuscript; available in PMC 2020 March 20.

Published in final edited form as:

ACS Appl Mater Interfaces. 2019 August 14; 11(32): 28740–28751. doi:10.1021/acsami.9b10379.

Large-scale and rapid preparation of nanofibrous meshes and their application for drug-loaded multilayer mucoadhesive patch fabrication for mouth ulcer treatment

Liang Wei[†,§,⊥,‡], **Shaohua Wu**[⊥,‖,‡], **Wen Shi**[⊥], **Amy L. Aldrich**[▽], **Tammy Kielian**[▽], **Mark A. Carlson**[○], **Runjun Sun**[†], **Xiaohong Qin**[*,§], **Bin Duan**[*,⊥,○,#]

[†]School of Textile Science and Engineering, Xi'an Polytechnic University, Xi'an 710048, P. R. China

[§]Key Laboratory of Textile Science & Technology, Ministry of Education, College of Textiles, Donghua University, Shanghai 201620, P. R. China

[⊥]Mary & Dick Holland Regenerative Medicine Program; Division of Cardiology, Department of Internal Medicine, University of Nebraska Medical Center, Omaha, NE, 68198, USA

[‖]College of Textiles & Clothing, Qingdao University, Qingdao, 266071, P. R. China

[▽]Department of Pathology and Microbiology, University of Nebraska Medical Center, Omaha, NE, 68198, USA

[○]Department of Surgery, College of Medicine, University of Nebraska Medical Center, Omaha, NE, 68198, USA; Department of Surgery, VA Nebraska-Western Iowa Health Care System, Omaha, NE 68105, USA

[#]Department of Mechanical and Materials Engineering, University of Nebraska-Lincoln, Lincoln, NE, 68516, USA

Abstract

Electrospinning provides a simple and convenient method to fabricate nanofibrous meshes. However, the nanofiber productivity is often limited to laboratory scale, which cannot satisfy the requirements of practical application. In this study, we developed a novel needleless electrospinning spinneret based on a double ring slit to fabricate drug loaded nanofibrous meshes. In contrast to conventional single-needle electrospinning spinneret, our needless spinneret can significantly improve nanofiber productivity due to the simultaneous formation of multiple jets during electrospinning. Curcumin loaded poly (L-lactic acid) (PLLA) nanofiber meshes with various concentrations and large scale were manufactured by employing our developed needleless spinneret-based electrospinning device. We systematically investigated the drug release behaviors, antioxidant properties, anti-inflammatory attributes, and cytotoxicity of the curcumin loaded PLLA nanofibrous meshes. Furthermore, a bilayer nanofibrous composite mesh was successfully

[*]**Corresponding Authors:** xhqin@dhu.edu.cn, bin.duan@unmc.edu.

[‡]**Author Contributions:** Authors contributed equally.

Supporting Information

The Supporting Information is available on the website.

The authors declare no competing financial interest.

generated by electrospinning curcumin loaded PLLA solution and diclofenac sodium loaded poly(ethylene oxide) solution in a predetermined time sequence, which revealed potent anti-bacterial properties. Subsequently, novel mucoadhesive patches were assembled by combining the bilayer composite nanofibrous meshes with (hydroxypropyl)methyl cellulose-based mucoadhesive film. The multi-layered mucoadhesive patch had excellent adhesion properties on the porcine buccal mucosa. Overall, our double ring slit spinneret can provide a novel method to rapidly produce large scale drug-loaded nanofibrous meshes to fabricate mucoadhesive patches. The multiple layered mucoadhesive patches enable the incorporation of multiple drugs with different targets of action, such as analgesia, anti-inflammatory, and anti-microbial compounds, for mouth ulcer or other oral disease treatment.

Graphical Abstract

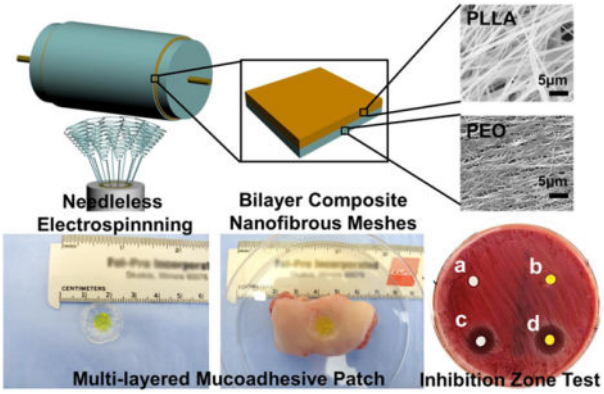

A novel needleless spinneret was developed to electrospun nanofibrous meshes with large-scale capacity and high productivity. This electrospinning setup supports multiple biomaterials and also enables fabrication of multilayered drug-loaded electrospun meshes. The multilayered mucoadhesive patches are fabricated as one example of biomedical application of this setup by combining the bilayer composite nanofibrous meshes with mucoadhesive film. Different drugs can be loaded into the nanofibrous meshes to achieve controlled and sequential drug release, anti-bacterial, antioxidant and anti-inflammatory properties. The multilayer mucoadhesive patches had a great potential for mouth ulcer or other oral disease treatment.

Keywords

needleless electrospinning; spinneret; nanofiber; mucoadhesive films; mouth ulcers

1. INTRODUCTION

Electrospinning has gained attention as a popular technique to fabricate nanofibrous materials, which shows promising applications for drug delivery[1–3], wound dressing[4–5], and engineered tissue scaffold[6]. Typical electrospinning setups are mainly based on single-needle spinneret (SNS). The limited nanofiber productivity of SNS-based electrospinning prevents the large-scale practical application. In addition, SNS is prone to clogging due to its small diameter, which has a negative effect on the continuity of spinning process. Recently,

needleless spinneret-based electrospinning has been regarded as an effective method, which can overcome the limitations of single-needle electrospinning, notably improving the nanofiber productivity and electrospinning continuity. Many needleless electrospinning spinnerets have been developed, which can fall into two categories based on spinning condition: rotary spinnerets and stationary spinnerets. Rotary spinnerets have spiral coil[7], rotary cone[8], sprocket wheel disk[9], needle-disk[10], rotating-disk[11], or self-cleaning threaded rod[12]. Stationary spinnerets include twisted wire[13], conical wire coil[14], metal dish[15], and tube[16]. The effects of spinning parameters on nanofiber morphology and diameter were investigated for these needleless electrospinning spinnerets. However, specific applications for the nanofibers prepared using these needleless spinnerets have rarely been reported. In addition, how to make full use of the polymer solution and reduce solvent volatilization during needleless electrospinning are also essential issues and are worthy of exploration.

Mouth ulcer or canker sore is one of the most common mouth diseases, which presents with inflammation of the oral mucosa and resultant pain[17–21]. About 2–5% of the total population suffers from mouth ulcers, and the clinically recommended treatment includes the use of topical antiseptic/anti-inflammatory agents[22]. Previous studies demonstrated that electrospun drug loaded nanofibrous meshes exhibited a porous structure and high specific surface area, which enabled the sustained release of an antiseptic/anti-inflammatory agent at the wound site in the mouth to treat oral diseases[23–24]. However, most studies loaded one drug into the electrospun monolayer nanofiber mesh, which likely cannot achieve optimal therapeutic effects for oral diseases. Ideally, multiple compounds should be sequentially delivered at different stages of disease, from eliminating bacterial infection to limiting the inflammatory response and oxidative stress, and finally to promote tissue regeneration[25–26]. Moreover, although some mucoadhesive polymeric nanofibers were electrospun and used for transmucosal drug delivery[27–28], their mucoadhesive capacity is much lower than that of commercial formulations based on cellulose derivatives[29–30]. Therefore, the combination of mucoadhesive film together with drug loaded nanofiber mesh(es) is probably a better strategy to treat mouth ulcers[31], which can not only achieve the appropriate sequence of drug release but also obtain superior mucoadhesive properties.

In this study, we developed a double-ring slit needleless spinneret (DRSNS) to fabricate nanofibrous meshes in a rapid and continuous manner and in large-scale. Moreover, our needleless spinneret could make full use of polymer solution and reduce solvent volatilization during electrospinning. We first investigated and compared the nanofiber productivity, morphology, and mechanical properties of electrospun poly (L-lactic acid) (PLLA) meshes fabricated by conventional SNS-based and our DRSNS-based electrospinning setup, respectively. We also explored the cell behaviors seeded on nanofibrous meshes fabricated by SNS and DRSNS-based setups. Then we employed our DRSNS-based electrospinning setup to manufacture various curcumin (CUR)-encapsulated PLLA nanofibrous meshes in a dose-dependent manner and investigated how CUR dosage affects the *in vitro* release behavior, cytotoxicity, and anti-inflammatory properties of nanofibrous meshes. We further generated multi-layered mucoadhesive patches by combining mucoadhesive film with bilayer composite nanofiber nanofibrous meshes constructed by CUR-loaded PLLA mesh and diclofenac sodium (DCS)-loaded poly

(ethylene oxide) (PEO) mesh. The adhesive force on the porcine mucosa and anti-bacterial properties of different drug-encapsulated meshes and patches were also measured.

2. EXPERIMENTAL SECTION

2.1 Design and Assembly of DRSNS-based electrospinning method

A novel needleless electrospinning setup was designed and assembled to facilitate the large-scale production of nanofibrous meshes (Fig. 1A). The setup has four main parts: DRSNS, syringe pump, high voltage generator and rotating metal cylinder collector. DRSNS was employed to generate multiple jets simultaneously, which could positively affect the nanofiber yield and ensure high efficiency. Briefly, the DRSNS was composed of four sections (i.e., shell, inner core, inner ring and outer ring), as shown in Fig. 1C. Polytetrafluoroethylene was utilized to manufacture the shell and inner core components, and copper was employed to construct both the inner and outer rings. The front and top view of our DRSNS are shown in Fig. 1D and E. The overall height and diameter of the DRSNS were 40 mm and 35 mm, respectively. The width of slit formed by the inner and outer rings was 0.5 mm. The DRSNS was placed in a pedestal and the polymer solution could be transported into the DRSNS slit using a solution supply tube through the pedestal. Similar to conventional electrospinning, a syringe pump was used to control the solution flow rate and supply polymer solutions for the DRSNS. A voltage supply was utilized to produce high voltage field, which supplied the driving force for the simultaneous formation of multiple jets on the DRSNS. The rotating metal cylinder collector with a controlled speed was employed to collect nanofibers. The DRSNS electrospinning process was presented in Supporting Information Video 1.

A typical laboratory-based electrospinning setup was also employed to fabricate nanofibrous meshes as control groups (Fig. 1B). SNS (18 G stainless steel needle) was employed to generate single jet. The internal and external diameter of SNS was 0.84 mm and 1.25 mm, respectively. Other parameters, including supply rate, voltage, and rotating speed, were the same as for DRSNS.

2.2 Preparation of PLLA nanofibrous meshes without or with drug encapsulation

PLLA, a commonly-used biopolymer, was employed as a model polymer to fabricate nanofibrous meshes by utilizing both DRSNS- and SNS-based setups. PLLA powder (Mw=100000g/mol, Jinan Daigang Biomaterial Co., Ltd) was dissolved into 1,1,1,3,3,3-Hexafluoro-2-propanol (HFIP, Acros Organics) to prepare the electrospinning solution at a concentration of 12% (w/v). A SNS-based setup was employed to electrospin both random and highly aligned PLLA nanofiber meshes (SNS-R and SNS-HA, respectively). A static aluminum plate collector was used to collect SNS-R, and the rotating speed was set to be 2305 r/min to collect SNS-HA. The applied voltage and collection distance were maintained at 15 kV and 12 cm, respectively. Meanwhile, we employed our novel DRSNS-based setup to manufacture PLLA nanofibrous meshes with both low and high alignment (DRSNS-LA and DRSNS-HA, respectively). The rotator speed was set to 689 r/min and 2305 r/min to collect DRSNS-LA and DRSNS-HA, respectively. The applied voltage and collection distance were fixed at 30 kV and 17 cm, respectively.

CUR (MP Biomedicals) was utilized as a model drug to fabricate drug loaded PLLA nanofibrous meshes using the DRSNS-based setup. CUR was dissolved in 12% (w/v) PLLA solution to achieve the different CUR concentrations of 0%, 0.04%, 0.4%, 4% (w/w, the weight ratio of CUR to PLLA) to be tested. The electrospinning parameters used were identical to the above-mentioned fabrication of pure PLLA nanofibrous meshes.

2.3 Morphological and mechanical characterization of the PLLA nanofibrous meshes

To observe the morphology of different PLLA nanofibrous meshes, samples were examined via a scanning electron microscope (SEM, FEI Quanta 200, Japan) after gold coating. The mean nanofiber diameter and standard deviation of approximately 50 nanofibers were determined using Image J software (NIH) based on the SEM images. The productivity of the SNS- versus DRSNS-based setups were determined by weighing PLLA nanofibrous mesh using an electronic balance. The mechanical properties of the different nanofibrous meshes were measured using a tensile strength tester (Shakopee, MN 55379). Samples were trimmed into rectangles of 30 mm × 5 mm. The tensile speed was 0.1 mm/s with the clamp distance of 10 mm and a pre-tension force of 0.1 cN.

2.4 Cell seeding and culture

Human adipose-derived mesenchymal stem cells (HADMSC, Lonza) were cultured in DMEM/F12 (Life Technologies), 10% fetal bovine serum, (FBS, Sigma Aldrich) and 1% penicillin/streptomycin (P/S, GE Healthcare Life Sciences). HADMSC were used between passages 4–6. Before cell seeding, PLLA nanofibrous meshes were punched into a 7 mm diameter circle, UV sterilized and immersed in 70% ethanol overnight, and washed three times in sterile phosphate-buffered saline (PBS) before incubating in growth medium overnight. A total of 1×10^5 HADMSCs were seeded onto PLLA nanofibrous meshes. For all cell culture experiments, HADMSCs were cultured in 5% CO_2 at 37 °C, and the medium was replaced every 2 days.

2.5 Cell viability

The viability of HADMSC seeded on different PLLA nanofibrous meshes was examined with Live/Dead staining assay[32–33] and MTT assay[34] at predetermined time points. The stained samples were observed using a confocal laser scanning microscope (CLSM) (LSM 710, Carl Zeiss). For MTT assay, the absorbance value was read at 540 nm using a microplate reader (Synergy H1, BioTek).

2.6 CUR release study

CUR loaded PLLA nanofibrous meshes (5 mg) were immersed in 1 ml sterile PBS with 0.5 % (v/v) TWEEN®20 (Sigma Aldrich) and placed in 12-well plates. To prevent PBS evaporation, plates were sealed with adhesive tape and placed in a 5% CO_2 at 37 °C atmosphere. At predetermined time points, the PBS solution was collected and stored at −80 °C to determine the kinetics of CUR release. The absorbance values of CUR release solution were read at 428 nm using a microplate reader.

2.7 Activation of monocytes and qPCR for inflammatory gene expression

Primary human monocytes (HM) were isolated from fresh, healthy human blood by using gradient centrifugation and were provided by UNMC Elutriation Core Facility. Effects of released CUR from PLLA nanofibers on inflammatory gene expression of activated HM were examined according to the following procedures. The PLLA nanofiber meshes containing different CUR concentrations were immersed in monocyte culture medium (RPMI-1640 from Gibco, with 10% FBS, 1% P/S) for 24 h, and these CUR released media were collected. HM were seeded in a 24-well plate at a cell density of 1×10^6 cells/ml, and pre-incubated for 1 h in CUR-free monocyte culture medium. Next, HMs were activated with 1 μg/ml lipopolysaccharide (LPS) to induce inflammatory gene expression. Then, the CUR-free medium was replaced with the above-mentioned CUR-conditioned media, and the activated HM were further cultured in different CUR released media for 3h.

Total RNA was extracted from the CUR-treated HM by using commercial QIA-Shredder and RNeasy mini kits (QIAgen)[33]. Total RNA was synthesized into first strand cDNA in a 20 μL reaction using an iScript cDNA synthesis kit (BioRad Laboratories). Real-time PCR analysis was performed in a StepOnePlus™ Real-Time PCR System (Thermo Scientific) using SsoAdvanced SYBR Green Supermix (Bio-Rad). cDNA samples were analyzed for genes of interest and for the housekeeping gene 18S rRNA. The level of expression of each target gene was calculated using the comparative Ct ($2^{-\Delta\Delta Ct}$) method. All primers used in this study are listed in Supporting Information Table S1.

2.8 Antioxidant activity test

The antioxidant activity of CUR-loaded PLLA nanofiber mesh was examined using a 2,2-diphenyl-1-picryl-hydrazyl-hydrate (DPPH) free radical assay[35]. In brief, DPPH (Alfa Aesar) was dissolved in methanol to prepare a 39.4 mg/L DPPH solution. 5 mg CUR loaded PLLA nanofiber meshes were placed into a 12-well plate, whereupon 3 ml DPPH solution was quickly added to immerse CUR loaded PLLA nanofiber meshes. The plate was covered using aluminum foil and the reaction solution was collected at pre-determined time points (i.e. 30 min, 60 min, 90 min, 120 min, 150 min, 180 min) to measure the absorbance at 517 nm using a microplate reader (Synergy H1, BioTek). DPPH solution alone was used as a control group. Antioxidant activity was calculated according to Equation (1):

$$\text{Antioxidant activity}\ (\%) = \frac{A_{control} - A_{sample}}{A_{control}} \times 100 \quad (1)$$

where $A_{control}$ and A_{sample} were the absorbance values of the control and sample groups, respectively.

2.9 Fabrication of multi-drug loaded bilayer composite meshes

To generate the multi-drug loaded bilayer composite mesh, we firstly employed our novel DRSNS-based setup to fabricate the CUR loaded PLLA nanofiber mesh as the bottom layer. Then, DCS (Alfa Aesar) loaded polyethylene-oxide (PEO, Mv=900000g/mol, Sigma Aldrich) nanofiber mesh was electrospun on the top layer of the CUR loaded PLLA nanofiber mesh. CUR loaded PLLA nanofiber mesh was fabricated by using above-

described 12% (w/v) PLLA solution with 4% (w/w) CUR addition. For the fabrication of DC loaded PEO nanofibrous mesh, PEO (0.25 g) powder was dissolved into deionized water (5 ml) to prepare a 5% (w/v) PEO solution, whereupon DCS (30% w/w to PEO) was added. The spinning time for both CUR loaded PLLA nanofiber mesh and DCS loaded PEO nanofiber mesh was set as 2 h.

2.10 Antibacterial test

A broth culture of *S. aureus* USA300 LAC13C was grown overnight at 37 °C in Brain Heart Infusion (BHI) medium and was used to make a lawn on blood agar plates[36]. At the time of inoculation, the nanofiber mesh was placed onto the bacteria covered blood agar plate. The plate was then incubated at 37 °C overnight and the zone of clearing was visualized. The zone of clearing was measured three times and the average diameter was calculated.

2.11 Fabrication of multi-layer mucoadhesive patch

Mucoadhesive film was prepared according to a previous report with some modification[37]. In brief, a mixture consisting of (hydroxypropyl)methyl cellulose (HPMC) (Viscosity 2600–5600 cp, Sigma Aldrich), propylene glycol (Fisher Chemical) and deionized water were stirred quickly to form homogeneous solution and centrifuged twice at 5,000 r/min to remove the bubbles. Next, the solution was transferred to a 10 ml syringe and slowly added to the circular silicone mold (16 mm in diameter and 1.5 mm in thickness). After 5 min, the multi-drug loaded bilayer nanofiber composite mesh (7 mm in diameter and 100 μm in thickness) was placed on the middle of the silicone mold. The multi-layer mucoadhesive patch was generated after air drying at room temperature for 24 h.

2.12 Adhesion force test

Fresh porcine buccal mucosa samples were harvested from euthanized domestic pigs (3–6 months-old; 35–70 kg) which had been on other protocols that did not affect the buccal mucosa. All protocols were approved by the Institutional Animal Care and Use Committee (IACUC) of the Omaha VA Medical Center and the University of Nebraska Medical Center (UNMC). Mucosal samples were harvested immediately after euthanasia, and then placed immediately into ice-cold saline. Tissue was kept at 4˚C and utilized within 12 h of harvest. The adhesion force between several different mesh (or patch) samples and porcine buccal mucosa was measured using an in-house testing device (Supporting Information Fig. S2). This device was comprised of an iron stand, fixed table, cotton yarn, two pulleys, and plastic dishes.

The porcine buccal mucosa tissue was sectioned into a rectangular shape with an approximate dimension of 3 cm × 2 cm × 2 cm (L × W × H). The multi-layer mucoadhesive patches or drug loaded electrospun meshes were applied to the porcine buccal mucosa tissue, which was fixed onto a cylindrical platform. The patches or meshes were pasted onto the bottom of a plastic dish. Water was slowly added to the other plastic dish until the meshes or patches were completely separated from the porcine buccal mucosa tissue. The adhesion force was calculated according to Equation (2):

$$\text{Adhesive force (N)} = \frac{w}{1000} \times 9.8 \quad (2)$$

Where w is the weight of added water.

2.13 H&E staining

Hematoxylin-eosin (H&E) staining was utilized to evaluate the interaction between the multi-layer mucoadhesive patch and porcine buccal mucosa. The multi-layer mucoadhesive patch was applied to the mucosa tissue and incubated for 4 h at 37°C, whereupon the patch-tissue construct was fixed using 4% paraformaldehyde at 4 °C for 24 h. After rinsing with PBS, the sample was immersed in a 30% (w/v) sucrose solution at 4 °C for 24 h and finally embedded into OTC. The patch-tissue construction was cryo-sectioned using a freezing microtome (Leica CM1950) and sections were stained by H&E and imaged using a stereomicroscope (SteREO Discovery. V8).

2.14 Statistical analysis

All quantitative data were expressed as mean ± standard deviation (SD). Pairwise comparisons between groups were conducted using an ANOVA with Scheffé post-hoc test. A value of $p < 0.05$ was considered statistically significant.

3. RESULTS

3.1 Morphologies of PLLA nanofibrous meshes fabricated by DRSNS- and SNS-based setups

Our novel DRSNS-based setup (Fig. 1A) was employed to fabricate PLLA nanofibrous meshes with both low and high fiber alignment (DRSNS-LA and DRSNS-HA, respectively). A traditional SNS-based electrospinning setup (Fig. 1B) was utilized to fabricate both randomly-oriented and highly aligned PLLA nanofibrous meshes (i.e., SNS-R and SNS-HA, respectively) as control groups. The jet formation process was totally different between the DRSNS-based setup and the SNS-based one. For the DRSNS-based setup, multiple jets were simultaneously developed along the circular slit between the inner and outer copper rings of the DRSNS. The reason could be explained that the polymer solution was limited to a narrow slit with a width of 0.5mm. When a high voltage was applied to the polymer solution, the solution surface became unstable under the action of the electric force. Meanwhile, some small wave-like movements could be observed on the solution surface. Once the electric force exceeded the joint action that originated from the solution's surface tension and viscous resistance, multiple jets could be ejected and produced from the solution's surface at the same time. For comparison, only one jet could be formed on the needle tip for the SNS-based setup. An 18G stainless steel needle was employed as the single needle spinneret, and the internal and external diameter of single needle was 0.84 mm and 1.25 mm, respectively. Due to the small size of the needle, very little polymer solution could be squeezed out of needle at the same time. Therefore, only one jet could be generated in the SNS-based setup.

We further compared the nanofiber productivity between our novel DRSNS-based setup and the traditional SNS-based setup, and some related quantitative data was shown in Figure 1F. The results showed that our DRSNS-based setup could significantly improve the nanofiber productivity, compared with the SNS-based setup (2.25±0.25 g/h for DRSNS vs. 0.1±0.03 g/h for SNS, roughly 22 times, $p<0.01$). Moreover, a wide range of polymers, such as polyacrylonitrile, polyvinyl alcohol, poly(methyl methacrylate), poly-DL-lactic acid and polycaprolactone, were successfully electrospun into nanofibers by using our DRSNS-based setup (Supporting Information Fig. S1), which demonstrated the versatility and feasibility of our novel designed electrospinning system.

The SEM images of SNS-R, SNS-HA, DRSNS-LA, and DRSNS-HA are presented in Fig. 2A–D. We found that all four PLLA meshes exhibited bead-free fibrous morphology and structure. The average nanofiber diameter was 689.3±194.6 nm for SNS-R (Fig. 2A) and 440.9±269.4 nm for SNS-HA (Fig. 2B). When implementing the DRSNS-based setup, although we utilized the lowest rotating speed, fiber alignment was still observed, to some extent, for DRSNS-LA (Fig. 2C). PLLA nanofibers fabricated by the DRSNS-based setup yielded larger average diameters (718.0±286.8 nm for DRSNS-LA and 780.5±319.9 nm for DRSNS-HA) compared with those fabricated by the SNS-based setup. The insert images of Fig. 2A–D depict the nanofiber diameter distribution. The nanofibers fabricated by SNS exhibited a narrow diameter distribution compared to those fabricated by DRSNS.

3.2 PLLA nanofibrous meshes fabricated by DRSNS-based setup displayed significantly enhanced mechanical properties

Uniaxial tensile results of four different PLLA nanofibrous meshes fabricated via DRSNS- and SNS-based setups are shown in Fig. 3A–D. As expected, the mesh with random fiber structure (SNS-R) showed homogenous mechanical properties with comparable stress, elongation, and elastic modulus in both directions. The aligned meshes fabricated by the SNS- and DRSNS-based setups at the aligned direction exhibited significantly higher stress and elastic modulus, but much lower elongation, as compared to those at the vertical direction (Fig. 3B–D). The nanofibrous meshes with high alignment fabricated by the DRSNS-based setup (DRSNS-HA) had much higher stress and elastic modulus compared to their counterparts fabricated by the SNS-based setup (SNS-HA). One reason for the improved mechanical properties is probably due to the increase of nanofiber diameters. In addition, the meshes fabricated by DRSNS-based setup may have a dense structure due to high productivity. These results demonstrated that the mechanical properties of the meshes were significantly dependent on the fiber alignment and fiber fabrication device. Moreover, our DRSNS-based setup could improve the mechanical properties of as-obtained PLLA nanofibrous meshes.

3.3 PLLA nanofibrous meshes fabricated by DRSNS-based setup support HADMSC viability and proliferation

A Live/Dead assay was conducted to evaluate the viability of HADMSCs seeded on four different PLLA nanofibrous meshes fabricated via the DRSNS- and SNS-based setups. We found that HADMSCs cultured on all four different PLLA meshes showed high viability (>95%) throughout 7 days of culture (Fig. 4A–D). HADMSCs cultured on SNS-R showed

random growth direction due to the random fiber structure in the SNS-R (Fig. 4A). SNS-HA with aligned nanofibers guided HADMSC growth along the orientation direction of nanofibers (Fig. 4B). The meshes fabricated by DRSNS with both low and high alignment (DRSNS-LA and DRSNS-HA, respectively) also guided HADMSC growth along the fiber alignment direction (Fig. 4C and D). MTT assays were performed as a quantitative measure of HADMSC proliferation (Fig. 4E). The results showed that HADMSCs had relatively slow growth and proliferation from day 1 to day 3. However, a significant increase of MTT absorbance was observed at day 7 for all the meshes. These results demonstrated that PLLA nanofibrous meshes fabricated by the DRSNS-based setup supported HADMSC viability, growth, alignment, and proliferation, similar to those fabricated by a typical SNS-based setup.

3.4 Fabrication and characterization of CUR loaded PLLA nanofibrous meshes by using DRSNS-based setup

SEM images of PLLA nanofibrous meshes loaded with different concentrations of CUR (0.04%, 0.4%, 4%, w/w) are shown in Fig. 5A–C. No significant differences were observed between the three different meshes; however, the fibers presented less-aligned morphology and structure compared to PLLA nanofibrous mesh without CUR encapsulation (Fig. 2D). This may be because the addition of CUR affects the PLLA solution properties and thus impacts the electrospinning process. Compared with the polymer solution without CUR, the CUR addition could change the conductivity of the whole polymer solution system, which further led to the change of charge distribution situation in the polymer jets under the high voltage electric field during electrospinning. Therefore, the finally-generated CUR-loaded nanofibrous meshes exhibited less-aligned morphology and structure. Fig. 5D shows the quantitative evaluation for HADMSC proliferation on different CUR loaded PLLA nanofiber meshes by MTT assay. No significant differences were observed between the meshes with 0, 0.04% and 0.4% CUR throughout the 7 days culture period. However, for the PLLA mesh with 4% CUR, the absorbance value was significantly higher than the other three groups. This likely resulted from increased absorbance readings by the higher CUR concentration, which was notably yellow when dissolved in dimethyl sulfoxide (DMSO). To further evaluate the effects of the high CUR dose on the viability and growth of HADMSCs, Live/Dead and Lactate dehydrogenase (LDH) assays were conducted (Supporting Information S1). HADMSCs seeded on PLLA nanofibrous mesh with and without 4% CUR showed comparable LDH release, indicating that CUR was not cytotoxic (Supporting Information Fig. S4). In addition, HADMSCs displayed a normal spreading morphology and high viability on the PLLA meshes with or without 4% CUR (Supporting Information Fig. S3).

Next, the release profiles of PLLA nanofibrous meshes with different CUR concentrations were examined. As shown in Fig. 5E, CUR loaded PLLA nanofibrous meshes displayed similar release kinetics with a relatively low initial burst and sustained release. Nanofibers loaded with 4% CUR exhibited a higher release rate than those containing 0.4% and 0.04% CUR. About 12 μg CUR was cumulatively released from 4% CUR loaded nanofiber mesh over a two-week period.

3.5 Anti-inflammatory and antioxidant activity of CUR released from PLLA nanofibrous meshes fabricated via a DRSNS-based setup

CUR is the active ingredient of turmeric and has been extensively studied because of its anti-cancer, anti-inflammatory, anti-oxidant, and anti-rheumatic properties, among others[38–41]. We first evaluated the anti-inflammatory effects of released CUR from CUR loaded PLLA nanofibrous meshes fabricated via DRSNS-based setup using human monocytes (HM). HM were activated by LPS and then treated with CUR released media for 3 h. RT-qPCR was employed to detect the relative expression of several pro-inflammatory genes, including CCL2, IFN-γ, TLR2, IL-6, and TNF-α (Fig. 6A). The results demonstrated that all concentrations of released CUR from PLLA meshes were capable of inhibiting inflammatory gene expression compared with no CUR treatment. IFN-γ and TNF-α expression were significantly decreased in all the CUR-treated groups, with monocytes exposed to the highest dose of CUR most significantly affected.

We next determined the antioxidant activity of PLLA nanofiber meshes with different CUR concentration using a DPPH assay (Fig. 6B). Antioxidants can transfer either an electron or hydrogen atom to DPPH to neutralize its free radical[42–43]. At the low concentration (0.04%), the released CUR showed limited free radical scavenging activity. In comparison, the nanofiber meshes with 4% CUR showed markedly higher antioxidant activity than those with 0.04% and 0.4% CUR at all the time points, demonstrating a dose-dependent effect on antioxidant activity. Moreover, the antioxidant activity gradually increased with extended incubation times, from inhibition of ~70% of DPPH at 30 min, to ~80% at 180 min for PLLA mesh with 4% CUR.

3.6 Fabrication of multi-drug loaded bilayer composite meshes and their antibacterial property

We next fabricated multi-drug loaded bilayer composite nanofibrous meshes using the DRSNS-based setup (Fig. 7A). We first electrospun PLLA nanofibrous mesh loaded with 4% CUR as the bottom layer, and then electrospun DCS loaded PEO nanofiber mesh on the top of CUR-loaded PLLA nanofibrous mesh (represented as the yellow and blue layers, respectively; Fig. 7A) to generate a bilayer composite mesh. The rationale for engineering a dual construct was because DCS is a non-steroidal anti-inflammatory drug, which has been shown to inhibit inflammation and pain in various animal models[44–45]. DCS exhibited beneficial effects for osteoarthritis[46], endodontic pain[47], actinic cheilitis, as well as antibacterial activity[48–49]. CUR could scavenge reaction oxygen radicals with its antioxidant property[50–51] and anti-inflammatory effects shown here (Fig. 6). The nanofibrous morphologies of CUR loaded PLLA mesh and DCS loaded PEO mesh are shown in Fig. 7A.

The antibacterial properties of the different bilayer composite meshes were investigated, by measuring zones of clearance of a *S. aureus* lawn (Fig. 7B). As expected, no antibacterial effects were observed for the bilayer composite meshes without drugs. The bilayer composite meshes with DCS showed obvious inhibition zones, demonstrating effective antibacterial activity against *S. aureus*. Interestingly, the bilayer composite mesh with CUR alone did not exhibit any antimicrobial effects. Quantification of the diameters of inhibition zone for bilayer composite meshes with DCS alone, and with both DCS and CUR, were

11.47 ± 0.19 mm and 12.33 ± 0.32 mm, respectively (Fig. 7C). These results demonstrated that DCS was the drug component responsible for the antibacterial activity of the bilayer composite meshes.

3.7 Fabrication of multi-layer mucoadhesive patch and its adhesive properties on porcine buccal mucosa

A multi-layer mucoadhesive patch was fabricated by stacking multi-drug loaded bilayer composite meshes with a HPMC-based mucoadhesive film (Fig. 8A). A photograph of the as-fabricated multi-layer mucoadhesive patch is presented in Fig. 8B. The surface and cross-section morphologies of the multi-layer mucoadhesive patch were observed by SEM (Fig. 8C and D). Based on the design, the diameter of the bilayer composite mesh was smaller than that of the mucoadhesive film, so the mucoadhesive film in the formed multi-layer patch could directly contact the buccal mucosa surface. The mucoadhesive film and multi-drug loaded bilayer composite mesh were well integrated without any delamination even after adhesion to the porcine buccal mucosa and further fixation and staining. Fig. 8E shows the photograph of a multi-layer mucoadhesive patch adhered to the porcine buccal mucosa. H&E staining showed that the multilayered patch formed intimate contacts with the surface of the buccal mucosa epithelium and no noticeable structural damage to the epithelium was observed. (Fig. 8F). Adhesion forces between the multi-layer mucoadhesive patch and the porcine buccal mucosa were measured using an in-house adhesion force testing device (Supporting Information Fig. S2). The lowest adhesion force (0.14 ± 0.01 N) was found between the CUR loaded PLLA nanofibrous mesh and porcine buccal mucosa. This is probably because PLLA is not a mucoadhesive polymer and has limited adhesive capacity (Fig. 8G). As expected, the force significantly increased with incorporation of the mucoadhesive film (0.32 ± 0.01 N). The multi-layer patch showed the highest force (0.6 ± 0.06 N), since PEO also has strong mucoadhesive properties. In addition, the PEO layer is partially dissolved upon contact with the moist mucosa, which may enhance the mucoadhesion. Collectively, these results demonstrated that the multi-layer patch had excellent mucoadhesive properties for future buccal administration and drug delivery.

4. DISCUSSION

SNS-based electrospinning has been widely utilized to prepare nanofibers in many research reports[1–3]. However, the major prevailing problems are that the nanofiber productivity fabricated by a SNS-based setup is very low and the SNS can easily clog. In contrast, needleless electrospinning spinnerets can overcome these deficiencies to fabricate nanofibrous meshes with higher quality and productivity. Over the past decades, several different needleless-based setups have been designed and implemented[52–53]. Normally, the spinneret of a needleless-based setup is a rotating metal roller which is submerged in a polymer solution[54]. One problem of this design is that solvent volatilization occurs and gradually affects the concentration of polymer spinning solution, resulting in a significantly positive influence on the normal spinning process. In addition, a large amount of solution is wasted after spinning. In the present work, we present the design and usage of a novel DRSNS approach. One important feature of our DRSNS is that the polymer solution can be limited into a circular narrow slit, and multiple jets can be formed concurrently along with

the circular narrow slit. Another feature of our DRSNS is that the polymer solution is transformed to a narrow slit from a syringe through a control pump, which reduces waste throughout the electrospinning process. Therefore, the structure of this spinneret can reduce the contact area between polymer solution and atmospheric environment and thus make full use of the polymer spinning solution.

In this study, we first systematically compared the properties of electrospun nanofibrous meshes fabricated using conventional SNS- and our DRSNS-based setups. We further demonstrated the feasibility of the implementation of DRSNS-based setup to fabricate multi-layered nanofibrous constructs with loading two different types of model drugs (i.e. curcumin and diclofenac sodium) and discussed their potential for mouth ulcer or other oral disease treatment. The PLLA meshes fabricated by the DRSNS-based setup presented larger fiber diameters, broader fiber diameter distribution, and higher mechanical properties, compared to their counterparts fabricated by the SNS-based setup. The reason may be attributed to the multiple jet formation at a high speed under a high voltage electric field for the DRSNS-based setup. Due to high electric force, more polymer solutions were concurrently stretched from the slit of the DRSNS and multiple jets were quickly collected on the rotating collector. The mechanical properties of PLLA nanofibrous meshes fabricated by the DRSNS-based setup were significantly increased because of larger nanofiber diameters and greater fiber alignment. With multiple jet formation and a fast fiber collection rate, the DRSNS-based setup can notably improve nanofiber productivity. More importantly, in comparison with the PLLA meshed fabricated by the SNS-based setup, the as-fabricated PLLA meshes by DRSNS-based setup had no adverse effects on HADMSC behavior and viability.

CUR has been incorporated into various electrospun nanofibrous meshes for wound healing[55–56] and local cancer treatment[57–58] due to its antioxidant, anti-inflammatory, and anti-tumor properties. Previous studies demonstrated that CUR inhibited TLR2 gene expression and function possibly via an oxidative process[59]. CUR loaded PCL nanofibers also dramatically reduced IL-6 production from LPS simulated macrophages[60]. Other studies also reported that CUR decreased IL-6, IL-8 and TNF-α expression by monocytes[61–62]. In our current study, we confirmed that CUR released from PLLA nanofibrous meshes fabricated by our DRSNS-based setup downregulated CCL2, IFN-ɣ, TLR2, IL-6, and TNFα expression in LPS-stimulated HM in a dose-dependent manner. Similarly, the antioxidant properties of the released CUR from PLLA meshes were also dose-dependent. The PLLA meshes with a higher CUR concentration (i.e. 4%) exhibited significantly more antioxidant activity compared to those with lower CUR doses. These results demonstrate that high CUR doses should be incorporated to achieve effective anti-inflammatory and antioxidant properties. However, the utilization of high CUR doses may negatively affect the viability and proliferation of normal cells[55, 63–64]. For example, Ranjbar-Mohammadi et al. demonstrated that meshes containing more than 5% CUR were cytotoxic[64]. Therefore, the appropriate CUR concentration (4%) used in the current study should be a well-balanced reference value for further clinical application.

For mouth ulcers or other oral diseases, a single drug therapy may not be an effective treatment. Multiple ulcers may appear simultaneously (i.e. a “crop” of ulcers) and may

persist because of inflammation and/or secondary infection. In addition, mouth ulcers are typically associated with significant pain. To address these issues, multi-drug loaded bilayer composite nanofibrous meshes composed of one layer of CUR loaded PLLA nanofiber mesh (CUR loading amount of 4%) and one layer of DCS loaded PEO nanofiber mesh (DCS loading amount of 30%) were fabricated using our DRSNS-based setup. A previous study showed that the application of DCS in hyaluronan could significantly reduce pain[65] and DCS loaded PEO nanofiber mesh also exhibited significant antibacterial properties. Therefore, the DCS loaded PEO nanofibrous mesh layer contacting the mouth ulcer could reduce pain and inhibit bacterial growth. We also stacked a CUR loaded PLLA nanofibrous mesh on top of this construct to further reduce inflammation.

Many different mucoadhesive patches have been reported in previous studies[37, 66–67]. In this work, a multi-layer mucoadhesive patch was successfully fabricated by assembling a CUR/DCS loaded bilayer composite mesh with a HPMC-based mucoadhesive film. Similarly to other studies, the drug loaded multi-layer mucoadhesive patch could firmly adhere to the porcine buccal mucosa tissue[68–69]. More importantly, the adhesion force for our mucoadhesive film incorporated CUR/DCS loaded bilayer composite mesh was notably higher compared with previous studies[68, 70]. The multi-layer mucoadhesive patch could better adhere to porcine buccal mucosa to ensure quick DCS release from the DCS loaded PEO nanofiber mesh concomitant with slow and sustained CUR release from CUR loaded PLLA nanofiber mesh, in order to deliver a combination of anti-inflammatory, antioxidant, and antibacterial properties and pain relief. This strategy provides a novel solution for treating mouth ulcers.

5. CONCLUSIONS

In summary, we successfully developed a novel DRSNS-based setup, which can prepare large-scale electrospun nanofibrous meshes for biomedical applications. We demonstrated that the PLLA nanofibrous meshes fabricated by our DRSNS-based setup did not adversely affect cell behaviors. In addition, the DRSNS-based setup supported the fabrication of drug loaded nanofibrous meshes, including CUR loaded PLLA and DCS loaded PEO. The PLLA nanofibrous meshes with a higher dose of CUR exhibited superior antioxidant and anti-inflammatory properties compared to lower doses. Furthermore, multi-layered mucoadhesive patches were fabricated by combining the bi-layered CUR loaded PLLA and DCS loaded PEO composite nanofibrous meshes with a HPMC-based mucoadhesive film. The multi-layered mucoadhesive patch showed excellent adhesive properties on the porcine buccal mucosa. The DRSNS-based setup has great potential for fabricating drug loaded nanofiber mesh with high productivity. The fabricated multi-layered mucoadhesive patch has multiple treatment effects that could be beneficial in the context of oral diseases, including anti-inflammatory, antioxidant, antibacterial properties, and pain relief.

Supplementary Material

Refer to Web version on PubMed Central for supplementary material.

Acknowledgements

This work is supported by the Chang Jiang Youth Scholars Program of China and grants (51773037 and 51373033) from the National Natural Science Foundation of China, Innovation Program of Shanghai Municipal Education Commission, Fundamental Research Funds for the Central Universities, and DHU Distinguished Young Professor Program to Dr. Xiaohong Qin; Chinese Universities Scientific Fund (CUSF-DH-D-2016008) and China Scholarship Council to Dr. Liang Wei; National Institutes of Health (R01 AR073225) to Dr. Bin Duan and (2P01AI083211) to Dr. Tammy Kielian.

ABBREVIATIONS

PLLA	poly (L-lactic acid)
SNS	single-needle spinneret
DRSNS	double-ring slit needleless spinneret
CUR	curcumin
DCS	diclofenac sodium
PEO	poly (ethylene oxide)
HFIP	1,1,1,3,3,3-Hexafluoro-2-propanol
SNS-R	single-needle spinneret random PLLA nanofiber meshes
SNS-HA	single-needle spinneret highly aligned PLLA nanofiber meshes
DRSNS-LA	double-ring slit needleless spinneret low alignment PLLA nanofiber meshes
DRSNS-HA	double-ring slit needleless spinneret high alignment PLLA nanofiber meshes
SEM	scanning electron microscope
HADMSC	human adipose-derived mesenchymal stem cells
FBS	fetal bovine serum
P/S	penicillin/streptomycin
PBS	phosphate-buffered saline
CLSM	confocal laser scanning microscope
HM	human monocytes
LPS	lipopolysaccharide
DPPH	2,2-diphenyl-1-picryl-hydrazyl-hydrate
BHI	brain heart infusion
HPMC	(hydroxypropyl)methyl cellulose

IACUC	Institutional Animal Care and Use Committee
UNMC	University of Nebraska Medical Center
H&E	hematoxylin-eosin
SD	standard deviation
LDH	lactate dehydrogenase
DMSO	dimethyl sulfoxide

REFERENCES

(1). Zeng J; Xu X; Chen X; Liang Q; Bian X; Yang L; Jing X Biodegradable electrospun fibers for drug delivery. Journal of controlled release 2003, 92 (3), 227–231. [PubMed: 14568403]

(2). Kim YJ; Ebara M; Aoyagi T A smart hyperthermia nanofiber with switchable drug release for inducing cancer apoptosis. Advanced Functional Materials 2013, 23 (46), 5753–5761.

(3). Yu D; Wang X; Li X; Chian W; Li Y; Liao Y Electrospun biphasic drug release polyvinylpyrrolidone/ethyl cellulose core/sheath nanofibers. Acta Biomaterialia 2013, 9 (3), 5665–5672. [PubMed: 23099302]

(4). Chen J-P; Chang G-Y; Chen J-K Electrospun collagen/chitosan nanofibrous membrane as wound dressing. Colloids and Surfaces A: Physicochemical and Engineering Aspects 2008, 313, 183–188.

(5). Cai Z.-x.; Mo X.-m.; Zhang K.-h.; Fan L.-p.; Yin A.-l.; He C.-l.; Wang H.-s. Fabrication of chitosan/silk fibroin composite nanofibers for wound-dressing applications. International journal of molecular sciences 2010, 11 (9), 3529–3539. [PubMed: 20957110]

(6). Barnes CP; Sell SA; Boland ED; Simpson DG; Bowlin GL Nanofiber technology: designing the next generation of tissue engineering scaffolds. Advanced drug delivery reviews 2007, 59 (14), 1413–1433. [PubMed: 17916396]

(7). Wang X; Niu H; Wang X; Lin T Needleless electrospinning of uniform nanofibers using spiral coil spinnerets. Journal of Nanomaterials 2012, 2012, 3.

(8). Lu B; Wang Y; Liu Y; Duan H; Zhou J; Zhang Z; Wang Y; Li X; Wang W; Lan W; Xie E Superhigh-throughput needleless electrospinning using a rotary cone as spinneret. Small 2010, 6 (15), 1612–6, DOI: 10.1002/smll.201000454. [PubMed: 20602427]

(9). Ali U; Niu H; Aslam S; Jabbar A; Rajput AW; Lin T Needleless electrospinning using sprocket wheel disk spinneret. Journal of Materials Science 2017, 52 (12), 7567–7577.

(10). Liu Z; Ang KKJ; He J Needle-disk electrospinning inspired by natural point discharge. Journal of Materials Science 2016, 52 (4), 1823–1830, DOI: 10.1007/s10853-016-0472-9.

(11). Ng J-J; Supaphol P Rotating-disk electrospinning: needleless electrospinning of poly(caprolactone), poly(lactic acid) and poly(vinyl alcohol) nanofiber mats with controlled morphology. Journal of Polymer Research 2018, 25 (7), DOI: 10.1007/s10965-018-1540-4.

(12). Zheng G; Jiang J; Wang X; Li W; Zhong W; Guo S Self-cleaning threaded rod spinneret for high-efficiency needleless electrospinning. Applied Physics A 2018, 124 (7), DOI: 10.1007/s00339-018-1892-y.

(13). Holopainen J; Penttinen T; Santala E; Ritala M Needleless electrospinning with twisted wire spinneret. Nanotechnology 2014, 26 (2), 025301. [PubMed: 25513842]

(14). Wang X; Xu W Effect of experimental parameters on needleless electrospinning from a conical wire coil. Journal of Applied Polymer Science 2012, 123 (6), 3703–3709, DOI: 10.1002/app.35044.

(15). Wei L; Yu H; Jia L; Qin X High-throughput nanofiber produced by needleless electrospinning using a metal dish as the spinneret. Textile Research Journal 2016, 88 (1), 80–88, DOI: 10.1177/0040517516677232.

(16). Jahan I; Wang L; Wang X Needleless Electrospinning from a Tube with an Embedded Wire Loop. Macromolecular Materials and Engineering 2018, 304 (3), 1800588, DOI: 10.1002/mame.201800588.

(17). Altenburg A; El-Haj N; Micheli C; Puttkammer M; Abdel-Naser MB; Zouboulis CC The treatment of chronic recurrent oral aphthous ulcers. Deutsches Ärzteblatt International 2014, 111 (40), 665. [PubMed: 25346356]

(18). Hopper SM; McCarthy M; Tancharoen C; Lee KJ; Davidson A; Babl FE Topical lidocaine to improve oral intake in children with painful infectious mouth ulcers: a blinded, randomized, placebo-controlled trial. Annals of emergency medicine 2014, 63 (3), 292–299. [PubMed: 24210368]

(19). Sakly A; De Wever B; Jutla B; Satia M; Bogaert JP The safety and efficacy of AphtoFix® mouth ulcer cream in the management of recurrent aphthous stomatitis. BMC oral health 2016, 16 (1), 17. [PubMed: 26868504]

(20). Grimaux X; Leducq S; Goupille P; Aubourg A; Miquelestorena-Standley E; Samimi M Aphthous mouth ulcers as an initial manifestation of secukinumab-induced inflammatory bowel disease. Annales De Dermatologie Et De Venereologie 2018, 145 (11), 676–682, DOI: 10.1016/j.annder.2018.07.009. [PubMed: 30366718]

(21). Janse van Rensburg B; Freeman CR; Ford PJ; Taing M-W Investigating the management of potentially cancerous nonhealing mouth ulcers in Australian community pharmacies. Health & social care in the community 2019, 27 (2), 415–423, DOI: 10.1111/hsc.12661. [PubMed: 30246463]

(22). Kaur S; Chhabra M RECENT ADVANCEMENTS IN MOUTH ULCERS TREATMENT. International Journal of Pharmacology and Biological Sciences 2017, 11 (1), 45.

(23). Reda RI; Wen MM; El-Kamel AH Ketoprofen-loaded eudragit electrospun nanofibers for the treatment of oral mucositis. International journal of nanomedicine 2017, 12, 2335. [PubMed: 28392691]

(24). Aduba DC Jr; Hammer JA; Yuan Q; Yeudall WA; Bowlin GL; Yang H Semi-interpenetrating network (sIPN) gelatin nanofiber scaffolds for oral mucosal drug delivery. Acta biomaterialia 2013, 9 (5), 6576–6584. [PubMed: 23416578]

(25). Sundararaj SC; Thomas MV; Peyyala R; Dziubla TD; Puleo DA Design of a multiple drug delivery system directed at periodontitis. Biomaterials 2013, 34 (34), 8835–8842. [PubMed: 23948165]

(26). Gadde S Multi-drug delivery nanocarriers for combination therapy. MedChemComm 2015, 6 (11), 1916–1929.

(27). Singh H; Sharma R; Joshi M; Garg T; Goyal AK; Rath G Transmucosal delivery of Docetaxel by mucoadhesive polymeric nanofibers. Artificial cells, nanomedicine, and biotechnology 2015, 43 (4), 263–269.

(28). Zong S; Wang X; Yang Y; Wu W; Li H; Ma Y; Lin W; Sun T; Huang Y; Xie Z The use of cisplatin-loaded mucoadhesive nanofibers for local chemotherapy of cervical cancers in mice. European Journal of Pharmaceutics and Biopharmaceutics 2015, 93, 127–135. [PubMed: 25843238]

(29). Sudheer P Mucoadhesive Polymers: A Review. Journal of Pharmaceutical Research 2018, 17 (1), 47–55.

(30). Cook MT; Khutoryanskiy VV Mucoadhesion and mucosa-mimetic materials—A mini-review. International journal of pharmaceutics 2015, 495 (2), 991–998. [PubMed: 26440734]

(31). Masek J; Lubasova D; Lukac R; Turanek-Knotigova P; Kulich P; Plockova J; Maskova E; Prochazka L; Koudelka S; Sasithorn N; Gombos J; Bartheldyova E; Hubatka F; Raska M; Miller AD; Turanek J Multi-layered nanofibrousmucoadhesive films for buccal and sublingual administration of drug-delivery and vaccination nanoparticles - important step towards effective mucosal vaccines. Journal of Controlled Release 2017, 249, 183–195, DOI: 10.1016/j.jconrel.2016.07.036. [PubMed: 27469472]

(32). Wu S; Duan B; Qin X; Butcher JT Living nano-micro fibrous woven fabric/hydrogel composite scaffolds for heart valve engineering. Acta biomaterialia 2017, 51, 89–100. [PubMed: 28110071]

(33). Wu S; Peng H; Li X; Streubel PN; Liu Y; Duan B Effect of scaffold morphology and cell co-culture on tenogenic differentiation of HADMSC on centrifugal melt electrospun poly (L−lactic acid) fibrous meshes. Biofabrication 2017, 9 (4), 044106. [PubMed: 29134948]

(34). Wu S; Wang Y; Streubel PN; Duan B Living nanofiber yarn-based woven biotextiles for tendon tissue engineering using cell tri-culture and mechanical stimulation. Acta biomaterialia 2017, 62, 102–115. [PubMed: 28864251]

(35). Aytac Z; Uyar T Core-shell nanofibers of curcumin/cyclodextrin inclusion complex and polylactic acid: Enhanced water solubility and slow release of curcumin. International journal of pharmaceutics 2017, 518 (1–2), 177–184. [PubMed: 28057465]

(36). Thurlow LR; Hanke ML; Fritz T; Angle A; Aldrich A; Williams SH; Engebretsen IL; Bayles KW; Horswill AR; Kielian T Staphylococcus aureus Biofilms Prevent Macrophage Phagocytosis and Attenuate Inflammation In Vivo. Journal of Immunology 2011, 186 (11), 6585–6596.

(37). Perioli L; Ambrogi V; Angelici F; Ricci M; Giovagnoli S; Capuccella M; Rossi C Development of mucoadhesive patches for buccal administration of ibuprofen. Journal of controlled release 2004, 99 (1), 73–82. [PubMed: 15342182]

(38). Jaiswal S; Mishra P Co-delivery of curcumin and serratiopeptidase in HeLa and MCF-7 cells through nanoparticles show improved anti-cancer activity. Materials Science & Engineering C-Materials for Biological Applications 2018, 92, 673–684, DOI: 10.1016/j.msec.2018.07.025.

(39). Boyanapalli SSS; Huang Y; Su ZY; Cheng D; Zhang CY; Guo Y; Rao R; Androulakis IP; Kong AN Pharmacokinetics and Pharmacodynamics of Curcumin in regulating anti-inflammatory and epigenetic gene expression. Biopharm. Drug Dispos 2018, 39 (6), 289–297, DOI: 10.1002/bdd.2136. [PubMed: 29870054]

(40). Aldebasi YH; Aly SM; Rahmani AH Therapeutic implications of curcumin in the prevention of diabetic retinopathy via modulation of anti-oxidant activity and genetic pathways. International journal of physiology, pathophysiology and pharmacology 2013, 5 (4), 194–202.

(41). Deodhar SD; Sethi R; Srimal RC Preliminary study on antirheumatic activity of curcumin (diferuloyl methane). The Indian journal of medical research 1980, 71, 632–4. [PubMed: 7390600]

(42). Hara K; Someya T; Sano K; Sagane Y; Watanabe T; Wijesekara RGS Antioxidant activities of traditional plants in Sri Lanka by DPPH free radical-scavenging assay. Data in brief 2018, 17, 870–875, DOI: 10.1016/j.dib.2018.02.013. [PubMed: 29516033]

(43). Zamani M; Delfani AM; Jabbari M Scavenging performance and antioxidant activity of gamma-alumina nanoparticles towards DPPH free radical: Spectroscopic and DFT-D studies. Spectrochimica Acta Part a-Molecular and Biomolecular Spectroscopy 2018, 201, 288–299, DOI: 10.1016/j.saa.2018.05.004.

(44). Willis J; Kendall M; Flinn R; Thornhill D; Welling P The pharmacokinetics of diclofenac sodium following intravenous and oral administration. European journal of clinical pharmacology 1979, 16 (6), 405–410. [PubMed: 527637]

(45). Todd PA; Sorkin EM Diclofenac sodium. Drugs 1988, 35 (3), 244–285. [PubMed: 3286213]

(46). Francio VT; Towery C; Davani S; Brown TL A Clinical Perspective of Oral Versus Topical Diclofenac Sodium in The Treatment of Osteoarthritis. Archives of Physical Medicine and Rehabilitation 2017, 98 (10), e24–e25.

(47). Jenarthanan S; Subbarao C Comparative evaluation of the efficacy of diclofenac sodium administered using different delivery routes in the management of endodontic pain: A randomized controlled clinical trial. Journal of conservative dentistry: JCD 2018, 21 (3), 297. [PubMed: 29899633]

(48). Dastidar SG; Ganguly K; Chaudhuri K; Chakrabarty A The anti-bacterial action of diclofenac shown by inhibition of DNA synthesis. International journal of antimicrobial agents 2000, 14 (3), 249–251. [PubMed: 10773497]

(49). Toncheva A; Paneva D; Manolova N; Rashkov I Electrospun poly (L-lactide) membranes containing a single drug or multiple drug system for antimicrobial wound dressings. Macromolecular research 2011, 19 (12), 1310–1319.

(50). Kunchandy E; Rao M Oxygen radical scavenging activity of curcumin. International Journal of Pharmaceutics 1990, 58 (3), 237–240.

(51). Deldar Y; Pilehvar-Soltanahmadi Y; Dadashpour M; Montazer Saheb S; Rahmati-Yamchi M; Zarghami N An in vitro examination of the antioxidant, cytoprotective and anti-inflammatory properties of chrysin-loaded nanofibrous mats for potential wound healing applications. Artificial cells, nanomedicine, and biotechnology 2018, 46 (4), 706–716.

(52). Jirsak O; Sysel P; Sanetrnik F; Hruza J; Chaloupek J Polyamic acid nanofibers produced by needleless electrospinning. Journal of Nanomaterials 2010, 2010, 49.

(53). Niu H; Lin T; Wang X Needleless electrospinning. I. A comparison of cylinder and disk nozzles. Journal of Applied Polymer Science 2009, 114 (6), 3524–3530.

(54). Dubsky M; Kubinova S; Sirc J; Voska L; Zajicek R; Zajicova A; Lesny P; Jirkovska A; Michalek J; Munzarova M; Holan V; Sykova E Nanofibers prepared by needleless electrospinning technology as scaffolds for wound healing. J Mater Sci Mater Med 2012, 23 (4), 931–41, DOI: 10.1007/s10856-012-4577-7. [PubMed: 22331377]

(55). Merrell JG; McLaughlin SW; Tie L; Laurencin CT; Chen AF; Nair LS Curcumin-loaded poly (ε-caprolactone) nanofibres: Diabetic wound dressing with anti-oxidant and anti-inflammatory properties. Clinical and Experimental Pharmacology and Physiology 2009, 36 (12), 1149–1156. [PubMed: 19473187]

(56). Bui HT; Chung OH; Dela Cruz J; Park JS Fabrication and characterization of electrospun curcumin-loaded polycaprolactone-polyethylene glycol nanofibers for enhanced wound healing. Macromolecular Research 2014, 22 (12), 1288–1296, DOI: 10.1007/s13233-014-2179-6.

(57). Wang C; Ma C; Wu ZK; Liang H; Yan P; Song J; Ma N; Zhao QH Enhanced Bioavailability and Anticancer Effect of Curcumin-Loaded Electrospun Nanofiber: In Vitro and In Vivo Study. Nanoscale Research Letters 2015, 10, 10, DOI: 10.1186/s11671-015-1146-2. [PubMed: 25852308]

(58). Guo G; Fu SZ; Zhou LX; Liang H; Fan M; Luo F; Qian ZY; Wei YQ Preparation of curcumin loaded poly(epsilon-caprolactone)-poly(ethylene glycol)-poly(epsilon-caprolactone) nanofibers and their in vitro antitumor activity against Glioma 9L cells. Nanoscale 2011, 3 (9), 3825–3832, DOI: 10.1039/c1nr10484e. [PubMed: 21847493]

(59). Shuto T; Ono T; Ohira Y; Shimasaki S; Mizunoe S; Watanabe K; Suico MA; Koga T; Sato T; Morino S Curcumin decreases toll-like receptor-2 gene expression and function in human monocytes and neutrophils. Biochemical and biophysical research communications 2010, 398 (4), 647–652. [PubMed: 20599422]

(60). Ma Q; Ren Y; Wang L Investigation of antioxidant activity and release kinetics of curcumin from tara gum/polyvinyl alcohol active film. Food Hydrocolloids 2017, 70, 286–292.

(61). Kloesch B; Gober L; Loebsch S; Vcelar B; Helson L; Steiner G In vitro study of a liposomal curcumin formulation (Lipocurc™): toxicity and biological activity in synovial fibroblasts and macrophages. in vivo 2016, 30 (4), 413–419. [PubMed: 27381602]

(62). ABE Y; Hashimoto S; HORIE T Curcumin inhibition of inflammatory cytokine production by human peripheral blood monocytes and alveolar macrophages. Pharmacological research 1999, 39 (1), 41–47. [PubMed: 10051376]

(63). Sampath M; Lakra R; Korrapati P; Sengottuvelan B Curcumin loaded poly (lactic-co-glycolic) acid nanofiber for the treatment of carcinoma. Colloids and Surfaces B-Biointerfaces 2014, 117, 128–134, DOI: 10.1016/j.colsurfb.2014.02.020.

(64). Ranjbar-Mohammadi M; Bahrami SH Electrospun curcumin loaded poly(epsilon-caprolactone)/gum tragacanth nanofibers for biomedical application. International Journal of Biological Macromolecules 2016, 84, 448–456, DOI: 10.1016/j.ijbiomac.2015.12.024. [PubMed: 26706845]

(65). Saxen MA; Ambrosius WT; Rehemtula al KF; Russell AL; Eckert GJ Sustained relief of oral aphthous ulcer pain from topical diclofenac in hyaluronan: a randomized, double-blind clinical trial. Oral surgery, oral medicine, oral pathology, oral radiology, and endodontics 1997, 84 (4), 356–61, DOI: 10.1016/s1079-2104(97)90031-7.

(66). Mura P; Corti G; Cirri M; Maestrelli F; Mennini N; Bragagni M Development of mucoadhesive films for buccal administration of flufenamic acid: effect of cyclodextrin complexation. Journal of pharmaceutical sciences 2010, 99 (7), 3019–3029. [PubMed: 20127823]

(67). Verma N; Chattopadhyay P Preparation of mucoadhesive patches for buccal administration of metoprolol succinate: in vitro and in vivo drug release and bioadhesion. Tropical Journal of Pharmaceutical Research 2012, 11 (1), 9–17.

(68). Shidhaye SS; Saindane NS; Sutar S; Kadam V Mucoadhesive bilayered patches for administration of sumatriptan succinate. AAPS PharmSciTech 2008, 9 (3), 909–916. [PubMed: 18679806]

(69). Santocildes-Romero ME; Hadley L; Clitherow KH; Hansen J; Murdoch C; Colley HE; Thornhill MH; Hatton PV Fabrication of electrospun mucoadhesive membranes for therapeutic applications in oral medicine. ACS applied materials & interfaces 2017, 9 (13), 11557–11567. [PubMed: 28299922]

(70). Mendes AC; Gorzelanny C; Halter N; Schneider SW; Chronakis IS Hybrid electrospun chitosan-phospholipids nanofibers for transdermal drug delivery. International journal of pharmaceutics 2016, 510 (1), 48–56. [PubMed: 27286632]

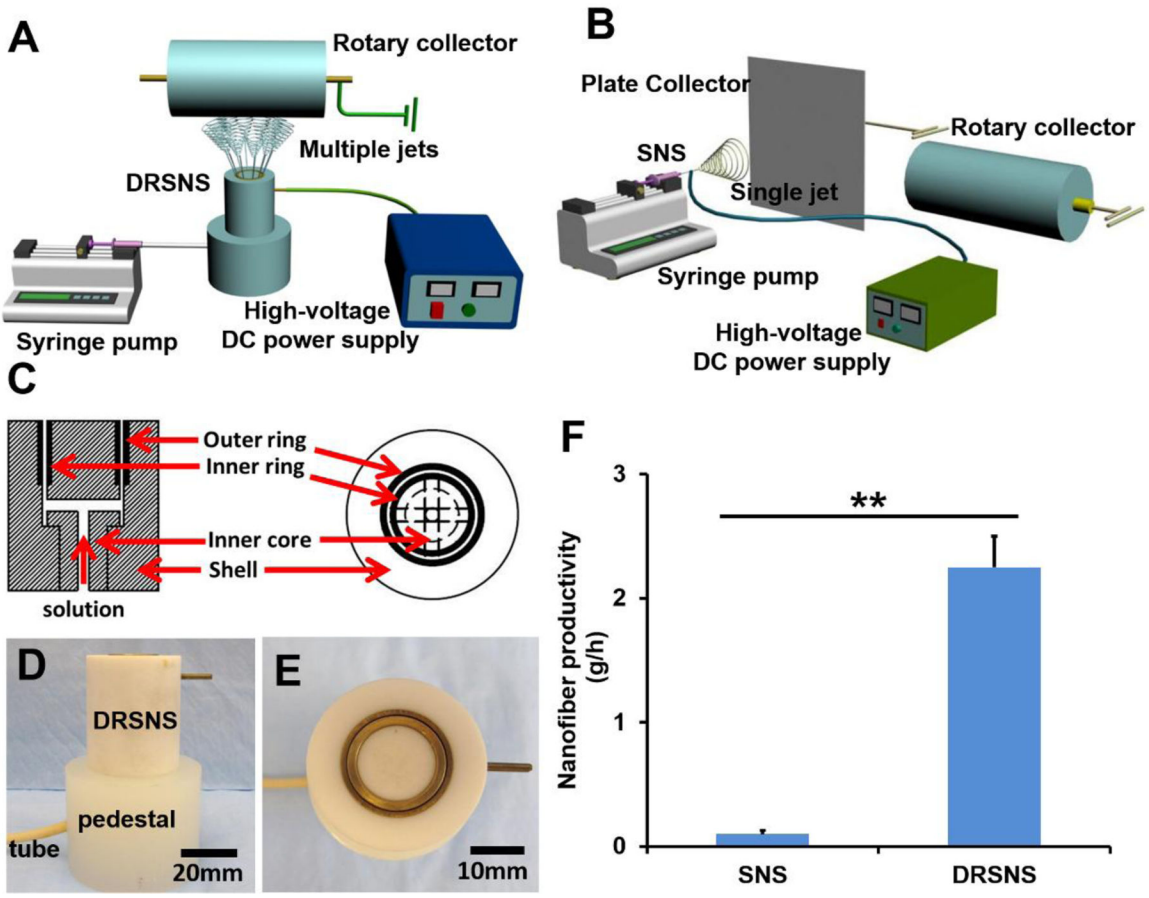

Figure 1.

Schematic of (A) DRSNS-based setup and (B) SNS-based setup (A plate collector was employed to fabricate randomly oriented nanofibrous meshes, and a rotary collector was utilized to fabricate highly aligned nanofibrous meshes); (C) Schematic of DRSNS internal structure; (D) Front view and (E) top view of DRSNS; (F) Calculation and comparison of nanofiber productivity fabricated by DRSNS and SNS (n=5; $^{**}p < 0.01$).

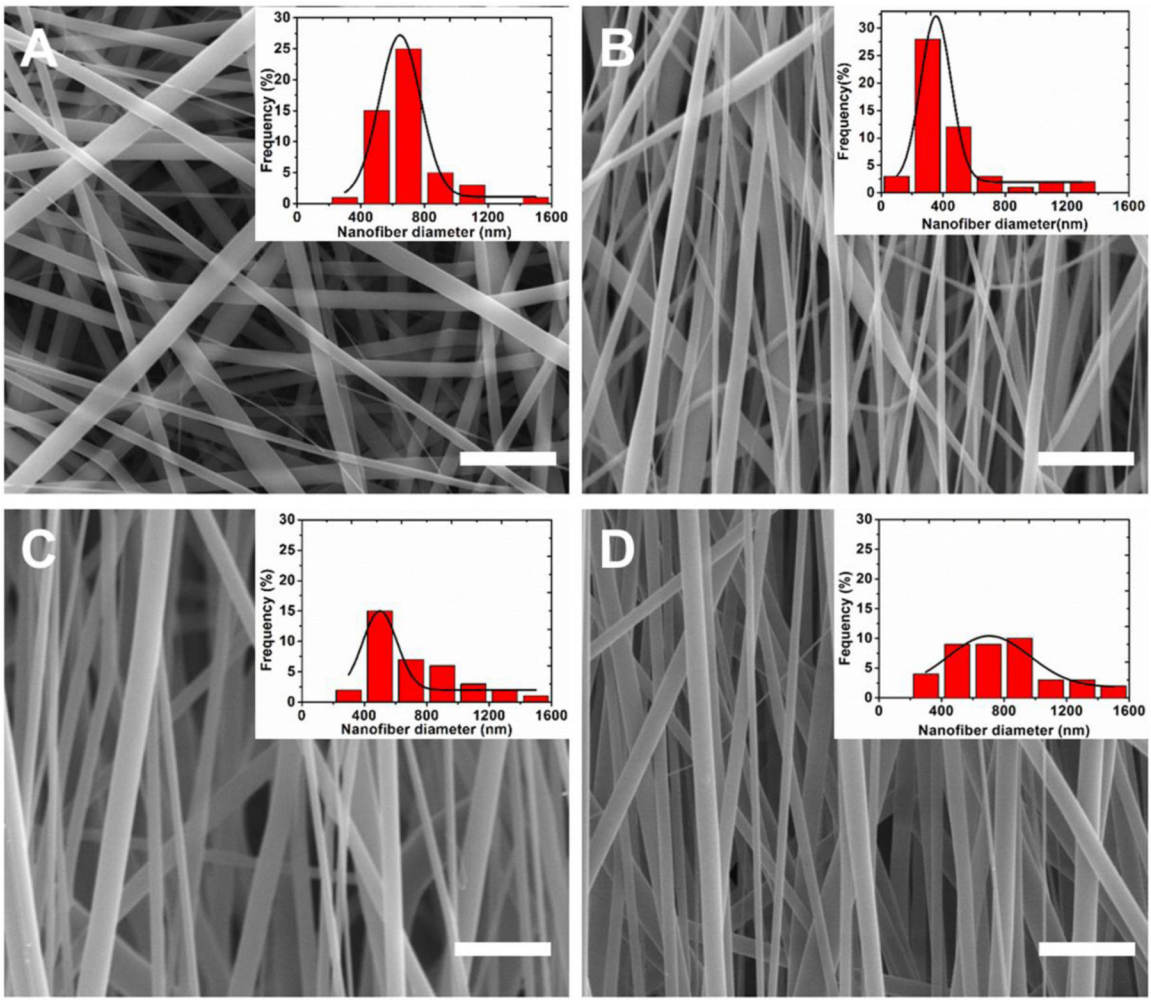

Figure 2.

SEM images of as-prepared PLLA nanofibrous meshes: (A) SNS-R, (B) SNS-HA, (C) DRSNS-LA and (D) DRSNS-HA. Insert images: the diameter distribution of nanofibers. Scale bar=5 μm.

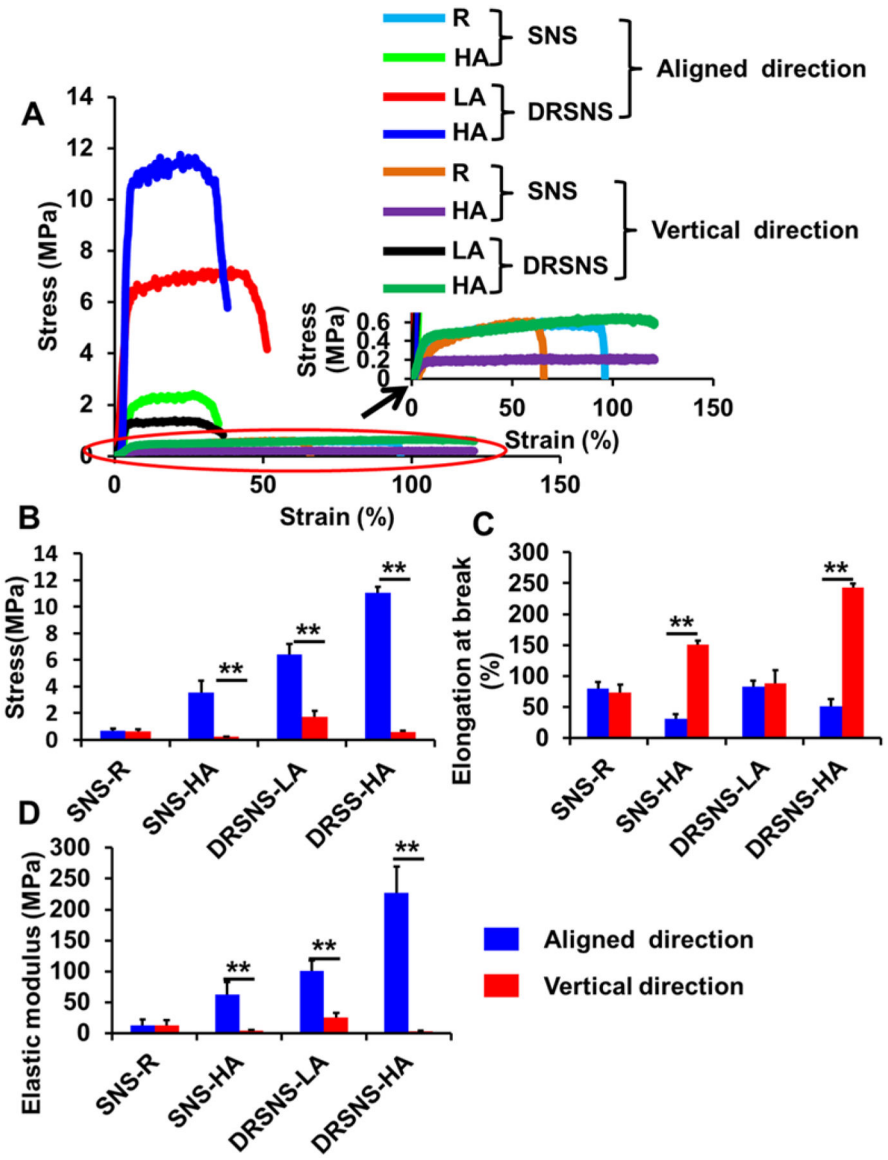

Figure 3.

Tensile mechanical properties of PLLA nanofibrous meshes fabricated using SNS- and DRSNS-based setups. (A) Typical strain-stress curves, (B) stress, (C) elongation at break, and (D) elastic modulus. (n=5; *p < 0.05, **p < 0.01).

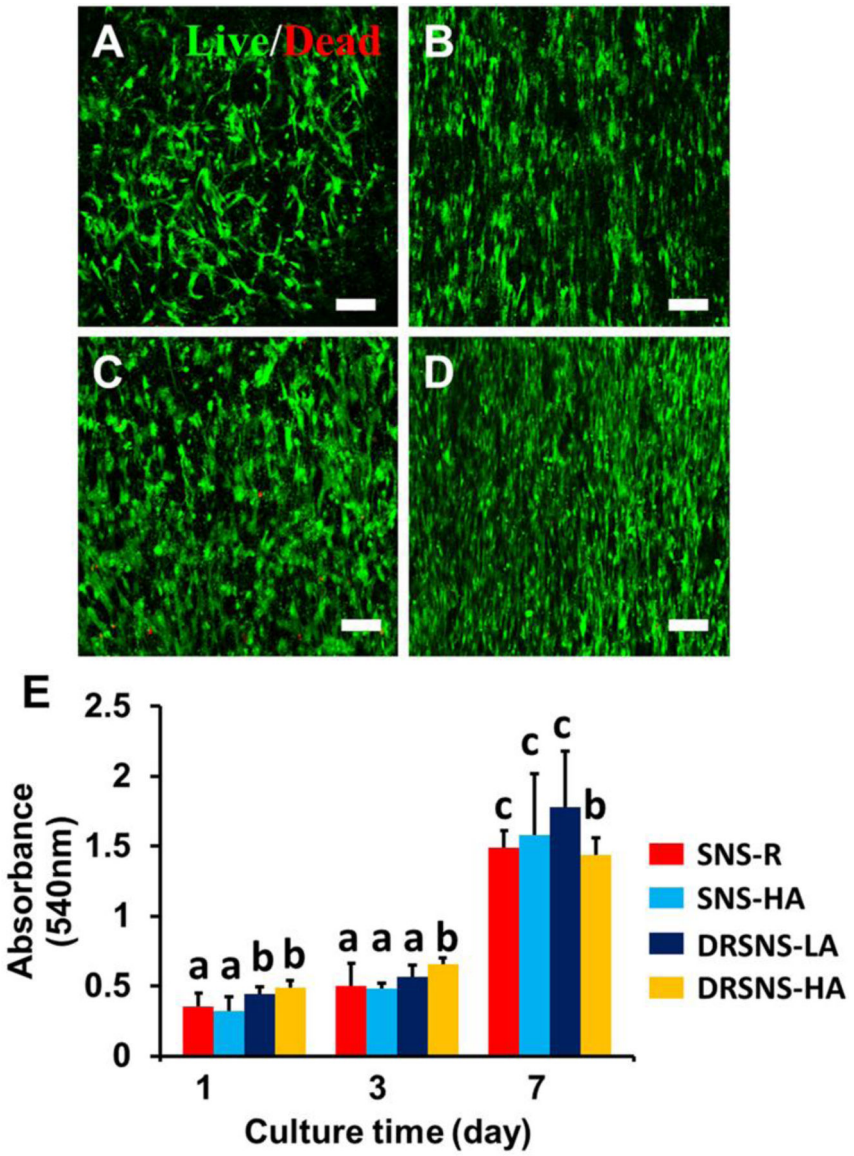

Figure 4.

HADMSC viability and proliferation on the four different PLLA meshes fabricated by SNS- and DRSNS-based setups. Live/Dead images of HADMSCs seeded on (A) SNS-R, (B) SNS-HA, (C) DRSNS-LA and (D) DRSNS-HA after 7 days of culture. Scale bar=100 μm. (E) Cell proliferation measured by MTT assay at days 1, 3 and 7 on the four different PLLA meshes populated with HADMSCs (n=6; bars that do not share letters are significantly different from each other; *$p < 0.05$, **$p < 0.01$).

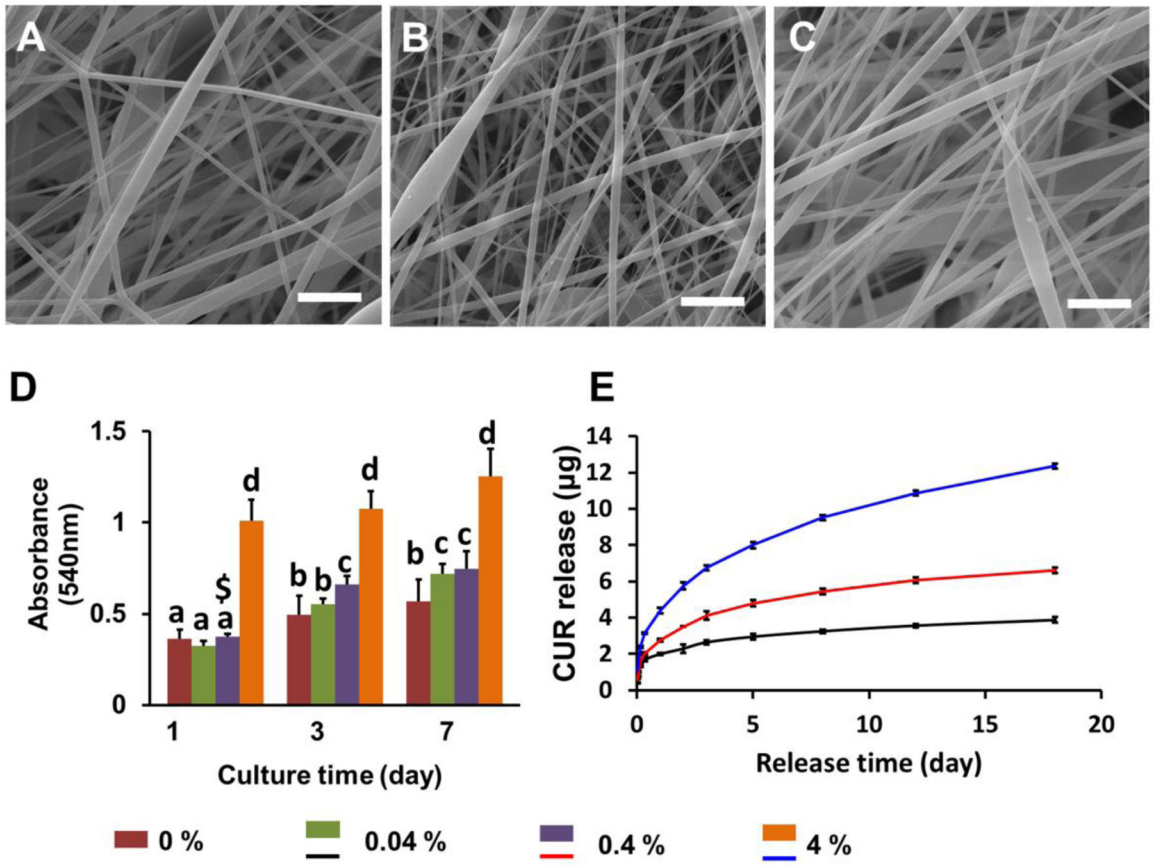

Figure 5.

Characterization of CUR loaded PLLA nanofibrous meshes. (A-C) SEM images of PLLA nanofibrous meshes loaded with (A) 0.04%, (B) 0.4% and (C) 4% CUR. Scale bar=5 μm; (D) Quantitative evaluation of HADMSC proliferation by MTT assay at 1, 3, and 7 days after seeding on PLLA nanofibrous meshes with different CUR concentrations; (E) CUR release profiles from the PLLA nanofibrous meshes with different CUR levels (n=6; bars that do not share letters are significantly different from each other; $ indicates significant difference between 0.04% and 0.4% at day 1; *$p < 0.05$, **$p < 0.01$).

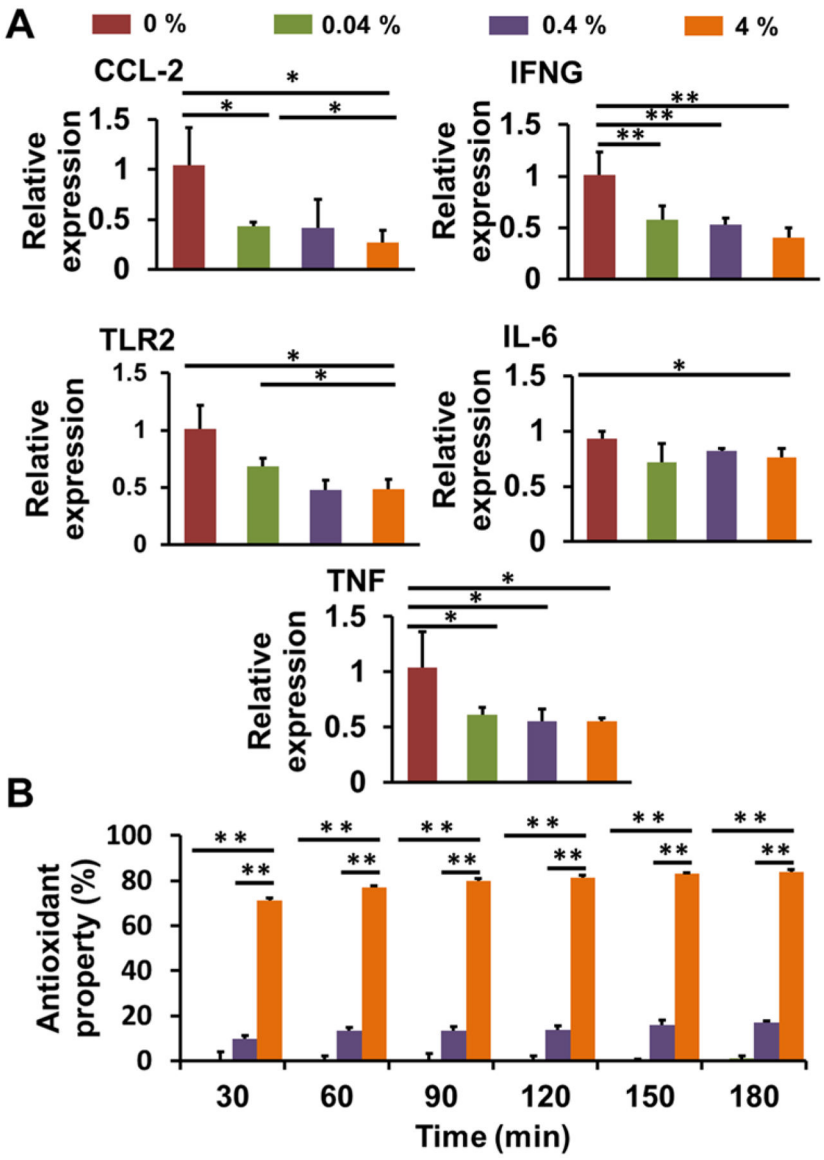

Figure 6.

Characterization of anti-inflammatory and antioxidant activities of CUR loaded PLLA nanofiber meshes fabricated via a DRSNS-based setup. (A) RT-qPCR analysis of inflammatory gene expression of LPS activated HM treated with different CUR released media. Relative gene expression was normalized to 18S, with results expressed relative to HM treated with medium without CUR. (n=3; *$p < 0.05$, **$p < 0.01$); (B) Antioxidant activity for different CUR loaded PLLA nanofiber meshes (n=6; *$p < 0.05$, **$p < 0.01$).

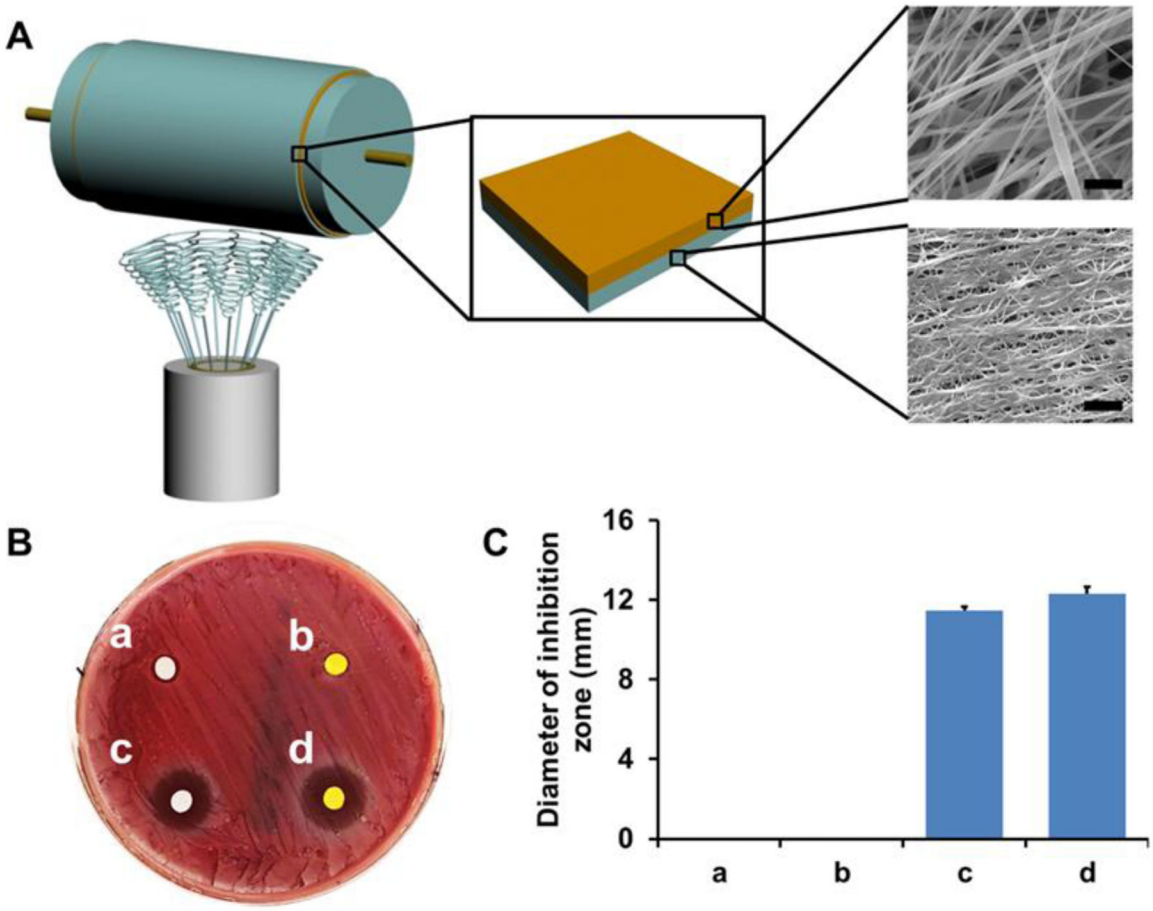

Figure 7.

Fabrication of multi-drug loaded bilayer composite meshes by using DRSNS-based setup and their antibacterial activity. (A) Schematic of multi-drug loaded bilayer composite meshes. Yellow layer: CUR loaded PLLA nanofibrous mesh; Blue layer DCS loaded PEO nanofibrous mesh. The morphology of each mesh was observed by SEM. Scale bar=5 μm; (B) Inhibition zone test for bilayer composite meshes without any drugs (a), with CUR alone (b), with DCS alone (c) and with both CUR and DCS (d) against *S. aureus*; (C) Average diameter calculation of inhibition zone of four different bilayer composite meshes.

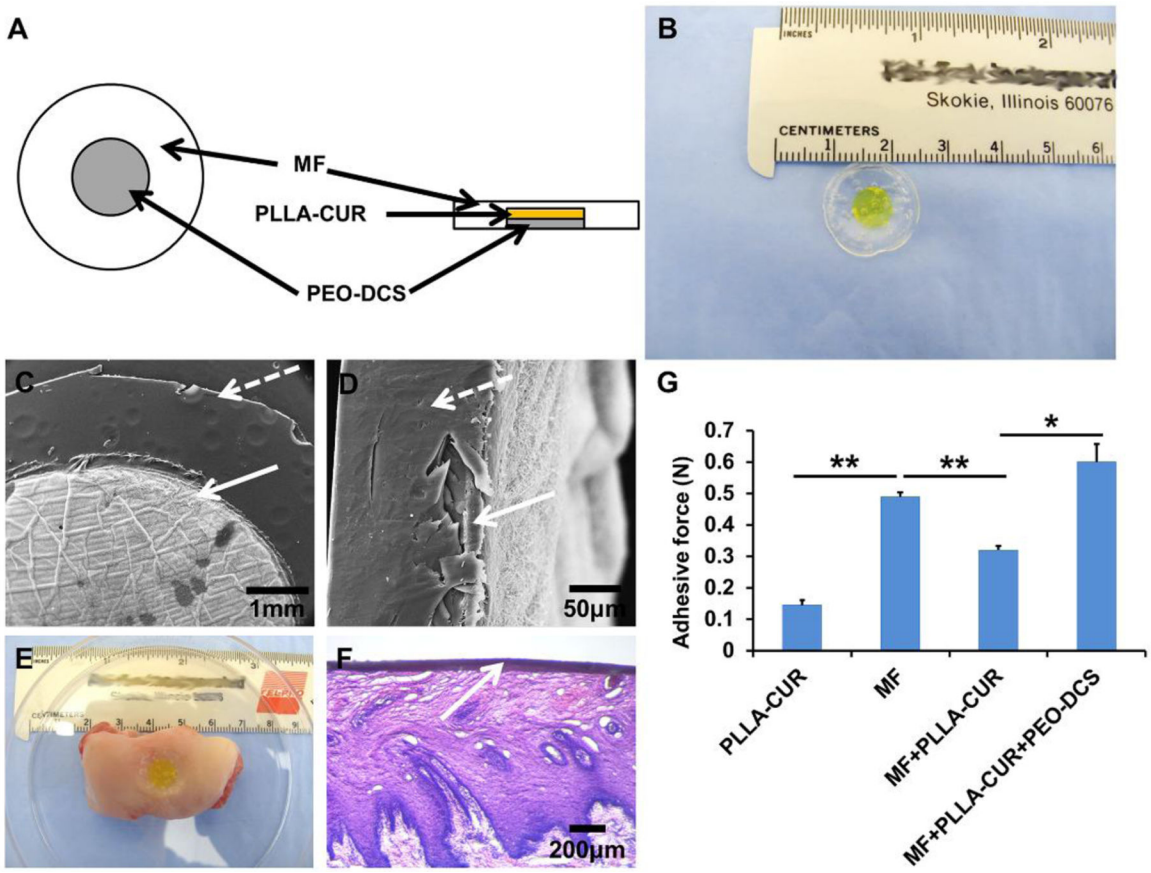

Figure 8.

Fabrication of a multi-layer mucoadhesive patch and its mucoadhesive properties on porcine buccal mucosa tissue. (A) Schematic of the multi-layer mucoadhesive patch structure; (B) Photograph of as-fabricated multi-layer mucoadhesive patch; SEM images of (C) surface morphology and (D) cross-section morphology; (E) A photograph of adhered multi-layer mucoadhesive patch on a section of porcine buccal mucosa; (F) H&E staining of multi-layer mucoadhesive patch adhered to the porcine buccal mucosa; (G) Mucoadhesive forces between different samples and porcine buccal mucosa (n=3; *p < 0.05, **p < 0.01).